

Quantum Criticality with Emergent Symmetry in the Extended Shastry-Sutherland Model

Wen-Yuan Liu,¹ Xiao-Tian Zhang,² Zhe Wang,³ Shou-Shu Gong,⁴ Wei-Qiang Chen,^{5,6} and Zheng-Cheng Gu⁷

¹*Division of Chemistry and Chemical Engineering, California Institute of Technology, Pasadena, California 91125, USA*

²*School of Physics, Beihang University, Beijing 100191, China*

³*Department of Physics, Beijing Normal University, Beijing 100875, China*

⁴*School of Physical Sciences, Great Bay University, Dongguan 523000, China, and
Great Bay Institute for Advanced Study, Dongguan 523000, China*

⁵*Institute for Quantum Science and Engineering and Department of Physics,
Southern University of Science and Technology, Shenzhen 518055, China*

⁶*Shenzhen Key Laboratory of Advanced Quantum Functional Materials and Devices,
Southern University of Science and Technology, Shenzhen 518055, China*

⁷*Department of Physics, The Chinese University of Hong Kong, Shatin, New Territories, Hong Kong, China
(Dated: May 31, 2024)*

Motivated by the novel phenomena observed in the layered material $\text{SrCu}_2(\text{BO}_3)_2$, the Shastry-Sutherland model (SSM) has been extensively studied as the minimal model for $\text{SrCu}_2(\text{BO}_3)_2$. However, the nature of its quantum phase transition from the plaquette valence-bond solid (PVBS) to antiferromagnetic (AFM) phase is under fierce debate, posing a challenge to understand the underlying quantum criticality. Via the state-of-the-art tensor network simulations, we study the ground state of the SSM on large-scale size up to 20×20 sites. We identify the continuous transition nature accompanied by an emergent $O(4)$ symmetry between the PVBS and AFM phase, which strongly suggests a deconfined quantum critical point (DQCP). Furthermore, we map out the phase diagram of an extended SSM that can be continuously tuned to the SSM, which demonstrates the same DQCP phenomena along a whole critical line. Our results indicate a compelling scenario for understanding the origin of the proposed proximate DQCP in recent experiments of $\text{SrCu}_2(\text{BO}_3)_2$.

Introduction. The frustrated Shastry-Sutherland magnet $\text{SrCu}_2(\text{BO}_3)_2$ is a fascinating material to explore exotic phenomena including magnetization plateaus, supersolid, and topological physics [1–16]. Recently, $\text{SrCu}_2(\text{BO}_3)_2$ has also attracted drastically increasing interest as a promising platform to experimentally study the physics of deconfined quantum critical point (DQCP) [17–20], which represents a new framework for understanding the unconventional continuous transitions beyond Landau-Ginzburg-Wilson paradigm and has been studied primarily through theoretical and numerical ways [21–48]. Remarkably, the recently observed magnetic field-driven PVBS-AFM transition in $\text{SrCu}_2(\text{BO}_3)_2$ displays extraordinary characteristics, including quantum critical scaling and emergence of $O(3)$ symmetry, that strongly suggests a nearby DQCP [49] and calls for theoretical understanding.

While the exact interactions for $\text{SrCu}_2(\text{BO}_3)_2$ are still unclear, most experimental observations can be understood based on the minimal Shastry-Sutherland model (SSM) [50, 51], with the following Hamiltonian:

$$H = J_1 \sum_{\langle i,j \rangle} \mathbf{S}_i \cdot \mathbf{S}_j + J_2 \sum_{\langle\langle i,j \rangle\rangle} \mathbf{S}_i \cdot \mathbf{S}_j, \quad (1)$$

where J_1 and J_2 terms sum over all the nearest-neighbor (NN) [gray lines in Fig. 1(b)] and part of the next-nearest-neighbor (NNN) AFM Heisenberg interactions [red dashed lines denoted as J_{2a} in Fig. 1(b)] on the square lattice. The model is in a dimer valence-bond solid (DVBS) phase for small J_1/J_2 and an AFM phase for large J_1/J_2 . The existence of a plaquette VBS phase (PVBS) between the DVBS and AFM phase has also been well established with a first-order DVBS-PVBS transition [19, 20, 49, 52–62]. Nevertheless, the transition nature between the PVBS and AFM phase, which is a promising candidate of DQCP and may play a crucial

role for understanding the proximate DQCP phenomena of $\text{SrCu}_2(\text{BO}_3)_2$ [19, 20, 49, 52, 54, 56–60, 62, 63], remains unresolved.

Specifically, whether the potential PVBS-AFM transition belongs to first order, a DQCP, or is extended to a gapless quantum spin liquid (QSL) phase in between is a big enigma. Series expansion study finds a continuous PVBS-AFM transition at $J_1/J_2 = 0.86(1)$ [63, 64], but infinite-size tensor network studies suggest a weakly first-order transition at $J_1/J_2 \approx 0.78$ [52, 56] and a multicritical point as a DQCP by introducing additional interactions [56]. In recent density matrix renormalization group (DMRG) studies, different conclusions have also been found. While an earlier study suggests a direct PVBS-AFM transition, which is further argued to represent a DQCP with emergent $O(4)$ symmetry based on quantum field theory analyses [54], a recent DMRG study based on gap crossings finds an intermediate gapless QSL phase between the PVBS and AFM phase for $0.79 \lesssim J_1/J_2 \lesssim 0.82$ [57]. This PVBS-QSL-AFM picture is also supported by a functional renormalization group study [58]. These controversial results lead to a big obstacle for further understanding of the proximate DQCP phenomena in $\text{SrCu}_2(\text{BO}_3)_2$ observed in a magnetic field and high pressure [49].

In this paper, we employ the state-of-the-art tensor network simulations by means of the finite projected entangled pair state (PEPS) approach to study an extended SSM with the following Hamiltonian:

$$H = J_1 \sum_{\langle i,j \rangle} \mathbf{S}_i \cdot \mathbf{S}_j + J_{2a} \sum_{\langle\langle i,j \rangle\rangle} \mathbf{S}_i \cdot \mathbf{S}_j + J_{2b} \sum_{\langle\langle i,j \rangle\rangle} \mathbf{S}_i \cdot \mathbf{S}_j, \quad (2)$$

where J_{2a} and J_{2b} represent two sets of the NNN interactions as shown in Fig. 1(b). For either $J_{2b} = 0$ or $J_{2a} = 0$, the model recovers the standard SSM, while for $J_{2a} = J_{2b}$ it is

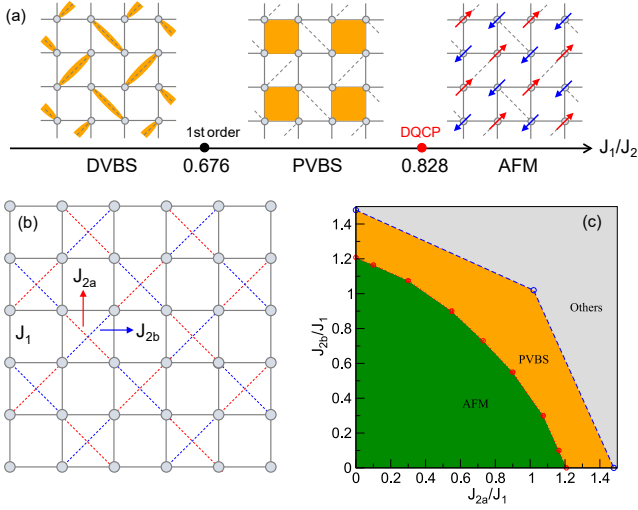


Figure 1. (a) Ground state phase diagram of the SSM, including three phase: DVBS, PVBS and AFM. Dashed diagonal lines indicate the NNN interaction terms. (b) The extended SSM, which contains two sets of NNN interaction J_{2a} (red) and J_{2b} (blue). (c) Ground state phase diagram of the extended Shastry-Sutherland model and it is symmetric about J_{2a} and J_{2b} . $J_{2b} = 0$ (or $J_{2a} = 0$) corresponds to the SSM, and $J_{2a} = J_{2b}$ corresponds to the checkerboard model (CBM). The grey region denotes other phases not of interest here.

the checkerboard model (CBM) with a potential PVBS-AFM transition [65–67]. The two models can be connected by tuning J_{2a} and J_{2b} . Our extensive tensor network simulations yield strong evidence that the SSM undergoes a direct PVBS-AFM transition accompanied by an emergent $O(4)$ symmetry, supporting a DQCP in the SSM. The conclusions are further strengthened by the investigations of the extended SSM, which exhibits the same type of DQCP physics as shown in the phase diagram Fig. 1(c). Our findings suggest an origin of the experimentally observed proximate DQCP phenomena in $\text{SrCu}_2(\text{BO}_3)_2$.

Results of the SSM. The finite PEPS algorithm here we adopt has been demonstrated as a powerful approach for simulating quantum spin systems [46–48, 68–70]. To further verify the finite PEPS results, we carefully compare with DMRG and infinite-size tensor network methods on the SSM [52, 56]. These results explicitly demonstrate the high accuracy of the finite PEPS method. (In addition, we also benchmark our results of $J-Q$ model with Quantum Monte Carlo simulation at all different sizes. See Supplemental Material [71].) We use $D = 8$ to perform all calculations, where both the ground state energy and order parameters are well converged for the largest available size 20×20 by very careful analysis for $D = 4 - 10$ results [71].

Since our method works well for open boundary systems, we first look into the boundary induced dimerized pattern on $L \times L$ systems for the SSM. We set $J_2 = 1$ to keep the same energy scale with previous studies. The local plaquette operator at site $\mathbf{i} = (i_x, i_y)$ is defined as $\Pi_{\mathbf{i}} = \frac{1}{2}(P_{\square, \mathbf{i}} + P_{\square, \mathbf{i}}^{-1})$, where $P_{\square, \mathbf{i}}$ denotes the cyclic exchange operator of the four spins on a given plaquette at site \mathbf{i} . The boundary

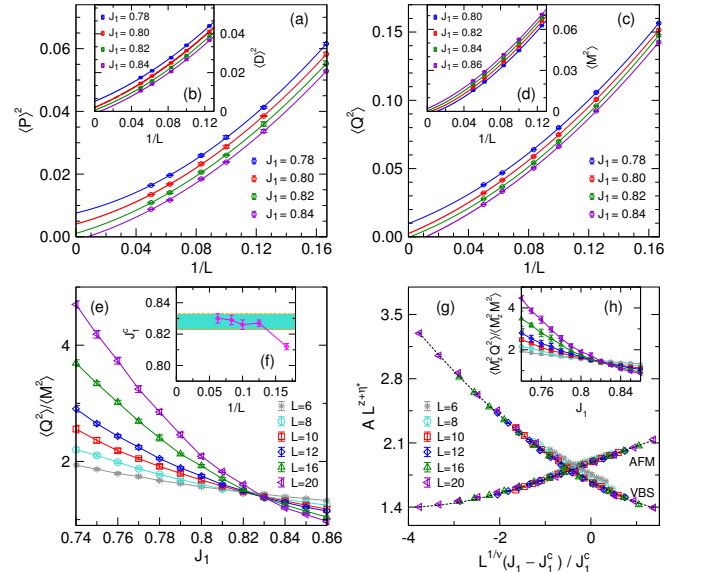


Figure 2. Finite size scaling of ground state order parameters for the SSM on $L \times L$ lattices (a)-(d). Quadratic fits are shown for VBS order parameters (a-c) and cubic fits are shown for AFM order parameter (d) using $L = 6 - 20$. The ratios of PVBS and AFM order parameters $\langle Q^2 \rangle / \langle M^2 \rangle$ are presented in (e) and their crossing points from $(L, L+2)$ or $(L, L+4)$ are presented in (f). (h) shows the fourth-order momentum ratio. (g) shows the data collapse of PVBS and AFM order parameters, and the dashed lines are quadratic curves using the corresponding critical exponents. The values of scaled AMF quantities in (g) have been shifted upwards by 0.7 for clear display.

induced plaquette order parameter is measured by $P = \frac{1}{N_p} \sum_{\mathbf{i}} (-1)^{i_x} \Pi_{\mathbf{i}}$, where $N_p = (L-1)^2$ is the total number of counted plaquettes [72]. The scaling of $\langle P \rangle^2$ with $L = 6 - 20$ is shown in Fig. 2(a) for different couplings J_1 using second order polynomial fits. With J_1 increasing, $\langle P \rangle^2$ gradually decreases. The extrapolated $\langle P \rangle^2$ in the thermodynamic limit at $J_1 = 0.78, 0.80, 0.82$ are 0.0075(3), 0.0041(3) and 0.0014(5), respectively, but would be zero at $J_1 = 0.84$. This suggests the PVBS phase vanishes around $J_1 = 0.83$. The third order fits give the same conclusion. The plaquette pattern in the PVBS phase is shown in the middle part of Fig. 1(a), where the singlets form on the empty plaquettes.

On the other hand, we consider the dimer order parameters for double check, defined as

$$D_{\alpha} = \frac{1}{N_b} \sum_{\mathbf{i}} (-1)^{i_{\alpha}} \mathbf{S}_{\mathbf{i}} \cdot \mathbf{S}_{\mathbf{i}+\mathbf{e}_{\alpha}}, \quad (3)$$

where $\alpha = x$ or y , and $N_b = L(L-1)$ is the corresponding total number of counted bonds along the α direction. For the PVBS phase, the boundary induced dimerization $\langle D \rangle^2 = \langle D_x \rangle^2 + \langle D_y \rangle^2$ should also be finite in the thermodynamic limit. The scaling of $\langle D \rangle^2$ for $J_1 = 0.78, 0.80, 0.82, 0.84$ using $L = 6 - 20$ is shown in Fig. 2(b), and indeed is consistent with a PVBS phase for $J_1 \lesssim 0.83$.

Now we turn to the PVBS and AFM order parameters defined based on correlation functions. The PVBS order

parameter is defined as $\langle Q^2 \rangle = \langle (D_x - D_y)^2 \rangle$ where $Q = D_x - D_y$ [54]. In Fig. 2(c), the quantity $\langle Q^2 \rangle$ is presented. The finite-size scaling shows $J_1 = 0.8$ has a nonzero PVBS order 0.0024(6) in the thermodynamic limit, and the vanishing point J_1 of PVBS order parameter is very close to that obtained from the scaling of boundary induced quantities $\langle P \rangle^2$ and $\langle D \rangle^2$. On the other hand, the AFM order parameter $\langle \mathbf{M}^2 \rangle$ where $\mathbf{M} = \frac{1}{L^2} \sum_i (-1)^{i_x+i_y} \mathbf{S}_i$ is show in Fig. 2(d). One can see with J_1 increasing, the AFM order increases, and potentially establishes for $J_1 \geq 0.84$. These results from different physical quantities suggest a direct PVBS-AFM phase transition. By using the crossing points of order parameter ratio, which we will mention later, it gives a PVBS-AFM transition point at $J_1 \simeq 0.83$, consistent with the finite size scaling analysis. The physical quantities vary smoothly about J_1 in our results, indicating a continuous PVBS-AFM transition, though the possibility of weakly first order transition in the thermodynamic limit can not be fully excluded.

The PVBS-AFM transition point in the SSM has been argued as a DQCP with emergent O(4) symmetry through the rotation of three components of AFM order parameter $\mathbf{M} = (M_x, M_y, M_z)$ and one-component PVBS order parameter Q into each other to form a superspin $\mathbf{n} = (M_x, M_y, M_z, Q)$, where $Q = D_x - D_y$ [54]. To check the O(4) symmetry, as we note the SO(3) symmetry for AFM components is well satisfied by observing $\langle M_\alpha^2 \rangle = \frac{1}{3} \langle \mathbf{M}^2 \rangle$ (see SM [71]), we only need to check the additional symmetry formed by M_z and Q . A simple but nontrivial quantity to verify the emergent O(4) symmetry is that the ratio $\langle Q^2 \rangle / \langle \mathbf{M}^2 \rangle$ (or $\langle Q^2 \rangle / \langle M_z^2 \rangle$ as $\langle M_z^2 \rangle = \frac{1}{3} \langle \mathbf{M}^2 \rangle$) should be size-independent at the transition point [30, 40, 73]. In Fig. 2(e), the quantities $\langle Q^2 \rangle / \langle \mathbf{M}^2 \rangle$ for different system size have a crossing point at $J_1 \simeq 0.83$, which is intrinsically close to the PVBS-AFM transition point evaluated by finite size scaling of order parameters. The crossing points show much smaller finite size effects [Fig. 2(f)], which has also been observed in other DQCP studies by Quantum Monte Carlo simulations [30, 40, 73]. These results on one hand provide direct evidence to support the PVBS-AFM transition point as a DQCP with emergent O(4) symmetry, on the other hand give a more accurate evaluation of the transition point $J_1^c = 0.828(5)$, significantly reducing the uncertainties from the finite size extrapolations of order parameters. We also consider higher order momentum ratios of order parameters to check the emergent symmetry [38, 40, 73], which is very challenging to compute. Within our capability, we can only get the fourth-order momentum ratio $\langle M_z^2 Q^2 \rangle / \langle M_z^2 \mathbf{M}^2 \rangle$. Remarkably, $\langle M_z^2 Q^2 \rangle / \langle M_z^2 \mathbf{M}^2 \rangle$ also has a crossing point around $J_1 \simeq 0.83$, shown in Fig. 2(h), further supporting the emergent symmetry.

The extensive data with different system size enable us to precisely extract the corresponding critical exponents. We use the standard finite size scaling formula without subleading corrections [74]:

$$A(J_1, L) = L^{-(z+\eta^*)} F[L^{1/\nu}(J_1 - J_1^c)/J_1^c], \quad (4)$$

where J_1 denotes the coupling constant, and $A(J_1, L)$ denote the AFM order parameters $\langle \mathbf{M}^2 \rangle$ or VBS order parameters

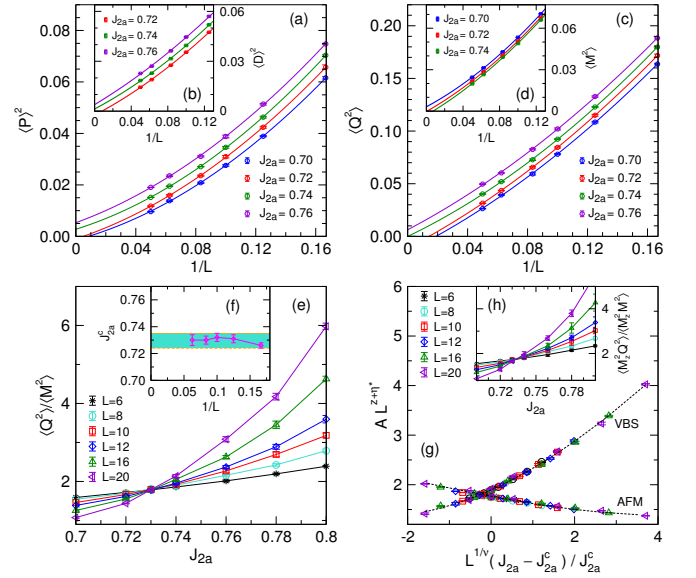


Figure 3. Finite size scaling of ground state order parameters for checkerboard model ($J_{2a} = J_{2b}$) on $L \times L$ lattices (a)-(d), setting $J_1 = 1$. Quadratic fits for $L = 6 - 20$ are shown. The meanings of the figures are the same with those of Fig. 2. The values of scaled AMF quantities in (g) have been shifted upwards by 0.7 for clear display.

$\langle Q^2 \rangle$ for different size L at different J_1 . ν is the correlation length exponent, and $z + \eta_{s,p}^*$ represents the spin or plaquette exponents where z is the dynamical exponent and $\eta_{s,p}^*$ are corresponding anomalous scaling dimensions. $F[x]$ is a polynomial function. The analysis of data collapse can be followed in Ref. [47]. In Fig. 2(g), we show the data collapse of the order parameters (using $J_1^c = 0.828$) by collectively fitting $A(J_1, L)$ with different J_1 and L (exclude $L = 6$), and the physical quantities can be well scaled with $z + \eta_s^* = 1.39(2)$, $z + \eta_p^* = 1.39(1)$ and $\nu = 0.84(3)$. On the other hand, note at the critical point $J_1 = J_1^c$ it has $A(J_1^c, L) \propto L^{-(z+\eta^*)}$, indicating that the exponents $(z + \eta^*)$ can be directly evaluated by using the data at J_1^c . Indeed at $J_1 = 0.83$ it gives the almost same value 1.39 for both $z + \eta_s^*$ and $z + \eta_p^*$, in good agreement with the collective fittings. Note that the obtained critical exponents clearly indicate $z + \eta_s^* = z + \eta_p^*$, which is consistent with the emergent O(4) symmetry [38, 48, 73].

At last, we compare our results with those from DMRG on smaller system size. Although converged DMRG results are unbiased, the limited system size and different analyzed quantities may lead to different conclusions for 2D limit. By computing the ground-state energy and correlation lengths on infinite-long cylinders, an earlier DMRG calculation finds a PVBS-AFM transition that can be consistent with an emergent O(4) symmetry. Nonetheless, a latter DMRG study using gap crossings suggests an intermediate QSL for $g_{c1} \lesssim J_1/J_2 \lesssim g_{c2}$ separating the PVBS and AFM phase in the SSM, where $g_{c1} \simeq 0.79$ and $g_{c2} \simeq 0.82$ are estimated from the $1/L^2$ finite-size scaling of gap crossings [57]. Notably, the extrapolated results based on the relatively small cylinder width near transition point may strongly depend on the assumed scaling formula [75]. Indeed, the extrapolated g_{c1} from linear fit

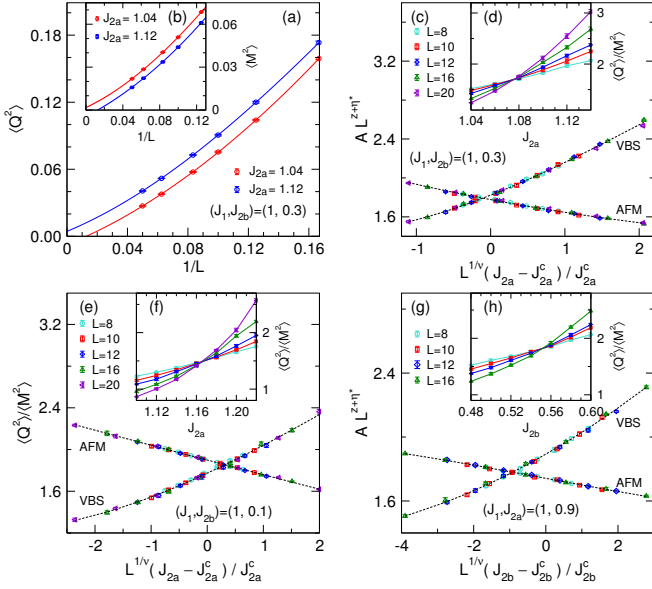


Figure 4. The scaling of AFM and VBS order parameters for three cases: $(J_1, J_{2b}) = (1, 0.3)$ with tuning parameter J_{2a} (a)-(d), and extrapolations with cubic fits for $L = 6 - 20$ are shown (a-b); $(J_1, J_{2b}) = (1, 0.1)$ with tuning parameter J_{2a} (e)-(f); and $(J_1, J_{2a}) = (1, 0.9)$ with tuning parameter J_{2b} (g)-(h). The values of scaled AMF quantities in (c), (e) and (g) have been shifted upwards by 0.7 for clear display.

of $1/L$, can become very close to the extrapolated g_{c2} (see SM [71]). Hence it is possible that g_{c1} and g_{c2} would eventually converge to the same value at larger size. Our extensive results, utilizing larger system sizes, reveal the emergence of $O(4)$ symmetry at the point $J_1^c = 0.828(5)$ in the SSM and similar features in the extended SSM, providing strong evidence for a direct PVBS-AFM transition and significantly diminishing the possibility of an intermediate QSL phase.

Results of the extended SSM. To gain more insight into the ground state phase diagram of SSM, we further consider the extended SSM Eq. (2), which is described by a two dimensional space of parameters $(J_{2a}/J_1, J_{2b}/J_1)$. For $J_{2b} = 0$ it recovers the SSM (relabel J_{2a} as J_2), and for $J_{2b} = J_{2a}$ it corresponds to the CBM. The two cases can be continuously connected by tuning the strength of J_{2b} terms. For the CBM, previous studies suggest it could have a direct PVBS-AFM transition [65–67]. Here we focus on the region close to the suggested PVBS-AFM transition. In Fig. 3, we present different quantities including boundary induced orders $\langle P \rangle^2$ and $\langle D \rangle^2$, and AFM and PVBS order parameters $\langle M^2 \rangle$ and $\langle Q^2 \rangle$, as well as the order parameter ratios, with the systems up to 20×20 sites. Similar to the analyses of the SSM, we find a continuous PVBS-AFM transition at $J_{2a}/J_1 = J_{2b}/J_1 \approx 0.73$ for the CBM, associated with the emergent $O(4)$ symmetry.

In fact, by computing the intermediate cases with proper J_{2a}/J_1 and J_{2b}/J_1 in between the SSM and the CBM, we find these different cases also support a continuous PVBS-AFM transition with emergent $O(4)$ symmetry. In Fig. 4, we present the scaling for the cases with fixed $J_{2a}/J_1 = 0.9$ (sweeping J_{2b}), fixed $J_{2b}/J_1 = 0.1$ (sweeping J_{2a}), as well as fixed

$J_{2b}/J_1 = 0.3$ (sweeping J_{2a}). In all of these cases, the PVBS has the same plaquette pattern with the SSM that the plaquette singlets are located on four sites without diagonal interaction terms [see Fig. 1(b)]. The extracted critical exponents for these different cases are given in Table I, and it clearly shows that the PVBS-AFM transitions have the similar critical exponents, $z + \eta_s^* = z + \eta_p^* \sim 1.35$ and $\nu \sim 0.80$, suggesting all of them belong to the same universality class. The same value of $z + \eta_s^*$ and $z + \eta_p^*$ is a reflection of the emergent $O(4)$ symmetry. Since the SSM can be smoothly connected to the CBM via the above intermediate cases, the results of extended SSM consolidate the existence of a DQCP.

Table I. Critical exponents of the extended SSM at the PVBS–AFM transition points. Critical points are from crossing points of the ratio of order parameters. Errors in critical exponents are from fittings.

model	$z + \eta_s^*$	$z + \eta_p^*$	ν	J_c
SSM [$J_{2a} = 1, J_{2b} = 0$]	1.39(2)	1.39(1)	0.84(3)	$J_1 = 0.828(5)$
CBM [$J_1 = 1, J_{2a} = J_{2b}$]	1.33(1)	1.33(1)	0.82(4)	$J_{2a} = 0.730(4)$
$(J_1, J_{2b}) = (1, 0.1)$	1.39(1)	1.39(1)	0.80(4)	$J_{2a} = 1.165(3)$
$(J_1, J_{2b}) = (1, 0.3)$	1.35(1)	1.35(1)	0.85(3)	$J_{2a} = 1.075(4)$
$(J_1, J_{2a}) = (1, 0.9)$	1.33(1)	1.33(1)	0.81(5)	$J_{2b} = 0.550(3)$

Summary and discussion. The nature of the PVBS-AFM transition in the SSM is a critical issue to be addressed. By applying the state-of-the-art finite-size tensor network simulations, we reveal a direct continuous PVBS-AFM transition in the SSM, accompanied by an emergent $O(4)$ symmetry. Further investigations on the extended SSM find the similar behaviors. These results are consistent with the DQCP nature of PVBS-AFM transition in the SSM, and exclude the existence of an intermediate QSL phase.

In the SSM, our PVBS-AFM transition point $J_1^c = 0.828(5)$ is a bit different from the one $J_1^c \approx 0.78$ obtained by the infinite-size tensor network simulations using a finite bond dimension D [52, 56]. This difference in principle could be further reduced by properly extrapolating the infinite-size results with a new finite correlation length scaling scenario or using a sufficiently large D [47, 76–79]. While the PVBS-AFM transition in our large-scale simulation is extremely close to a continuous transition, the possibility of a weakly first-order transition in the thermodynamic limit still cannot be fully excluded.

In the PVBS phase of $\text{SrCu}_2(\text{BO}_3)_2$, the plaquette singlets form at the sites with diagonal interactions, which is different from the SSM and is possibly owing to the weak intralayer and interlayer interactions [19, 20, 49, 53, 56, 62, 80, 81]. Interestingly, in the phase diagram of $\text{SrCu}_2(\text{BO}_3)_2$, including these extra interactions, the PVBS-AFM transition line in $\text{SrCu}_2(\text{BO}_3)_2$ still may connect the nearby DQCP in the SSM via a triple critical point [56], exhibiting large correlation lengths with emergent symmetry [54]. On the other hand, the PVBS in $\text{SrCu}_2(\text{BO}_3)_2$ also has two-fold degeneracy, which in presence of magnetic fields also naturally supports the observed $O(3)$ symmetry. Thus, our findings strongly suggest that it is a highly compelling scenario that the proximate DQCP phenomena observed in $\text{SrCu}_2(\text{BO}_3)_2$ under magnetic

fields, including the emergent $O(3)$ symmetry and quantum critical scaling at the PVBS-AFM transition [49], can originate from the DQCP universality class inherent in the SSM [54]. Consequently, the anomalous dimension scaling $\eta \sim 0.2$ under magnetic fields in $\text{SrCu}_2(\text{BO}_3)_2$ [49] is understandably near to our result $\eta \sim 0.35$ without magnetic fields (setting the dynamic exponent $z = 1$). Note that the SSM subjected to magnetic fields and additional interactions in $\text{SrCu}_2(\text{BO}_3)_2$, e.g., frustrated bilayer interaction $\sim 0.1J_2$, Dzyaloshinskii–Moriya interaction $\sim 0.03J_2$, and higher-order further-neighbour interaction [62, 80, 81], can possess very rich physics [6, 14, 15, 49, 60–62, 82–88], and we leave these interesting topics to future studies.

Acknowledgments. We thank Philippe Corboz, Wenan Guo, Wei Li, Frédéric Mila, Junsen Wang, Ning Xi, Zhi-Yuan Xie and Rong Yu for very helpful discussions. We also thank Philippe Corboz and Ning Xi for providing the iPEPS and iPESS data, respectively. This work was supported by the CRF C7012-21GF from the Hong Kong’s Research Grants Council, and the National Key R&D Program of China (Grants No. 2022YFA1403700). W.Q.C. was supported by the National Natural Science Foundation of China (Grants No. 12141402), the Science, Technology and Innovation Commission of Shenzhen Municipality (No. ZDSYS20190902092905285), and the Guangdong Basic and Applied Basic Research Foundation under Grant No. 2020B1515120100. This work was also granted access to the HPC resources of Center for Computational Science and Engineering at Southern University of Science and Technology. W.Y.L. was supported by the U.S. Department of Energy, Office of Science, National Quantum Information Science Research Centers, Quantum Systems Accelerator. X.T.Z. and S.S.G. were supported by the National Natural Science Foundation of China (No. 11874078 and No. 11834014), the Special Project in Key Areas for Universities in Guangdong Province (No. 2023ZDZX3054), and the Dongguan Key Laboratory of Artificial Intelligence Design for Advanced Materials. Z.W. was supported by the National Natural Science Foundation of China under Grant No. 12175015.

Supplemental Material

Appendix S-1: Tensor Network Method

The tensor network state, particularly the projected entangled pair state (PEPS), serves as a highly potent description for quantum many-body systems [89]. It has been extensively employed to characterize complex entangled many-body states, including those with topological order [90]. The expressive capacity of PEPS is systematically governed by the dimension D of tensors. In this study, we adopt the tensor network formalism using finite PEPS in the framework of variational Monte Carlo [68, 70], which works very well to deal with open boundary systems. This approach has proven very successful in elucidating the nature of particularly challenging frustrated spin systems [46–48]. The PEPS ansatz here we used is always defined on a square lattice with open boundaries. The tensors on the corners, edges and in the middle region, have 2, 3 and 4 virtual indices, respectively, to connect their nearest neighbour sites. Throughout this paper, unless otherwise specified, we use PEPS with $D = 8$ for all calculations which can provide well-converged results (see Sec. S-1.2). Here we show more results to further demonstrate the accuracy of our method.

1. comparison with QMC on $J - Q$ model

Here we present a comprehensive benchmark study on the spin-1/2 $J - Q$ model, also known as the Heisenberg model with additional four-spin exchange interactions [26]. This model can be unbiasedly simulated using quantum Monte Carlo (QMC) without encountering sign problems and served as a representative example for studying the DQCP [26]. The $J - Q$ model has a VBS-AFM phase transition at $J/Q = 0.0447(2)$ [91]. Due to the existence of four-spin interactions and critical properties for the $J - Q$ model, it thus also offers a highly nontrivial example to demonstrate the capability of PEPS to deal with critical systems.

Here we focus on two commonly studied near critical points: $J/Q = 0$ and $J/Q = 0.1$, which have very large correlation lengths around $\xi \sim 30$ [91]. The QMC results are obtained in the stochastic series expansion (SSE) method [74] on open boundary conditions, which operates in the S_z basis. In this context it is convenient to calculate the z -component quantities, including staggered magnetization $\langle M_z^2 \rangle = \frac{1}{N^2} \langle (\sum_i (-1)^{i_x+i_y} S_i^z)^2 \rangle$ where $N = L^2$, as well as the boundary-induced dimerization $\langle \bar{D} \rangle^2 = \frac{1}{2} (\langle \bar{D}_x \rangle^2 + \langle \bar{D}_y \rangle^2)$, where $\bar{D}_\alpha = \frac{1}{N_b} \sum_i (-1)^{i_\alpha} S_i^z S_{i+e_\alpha}^z$ with $N_b = L(L-1)$.

For the PEPS simulation, we use $D = 8$ PEPS as the variational ansatz, and stochastic gradient descent [68, 70] and stochastic reconfiguration [92] to optimize the PEPS wave function. After optimization, we can compute the physical quantities directly via Monte Carlo sampling of the optimized PEPS. Such energies can also be compared with the ones computed from the wave function by symmetrizing the optimized PEPS with horizontal and vertical lattice reflection

and spin inversion symmetry [70], which are listed in Table II. For $L = 20$, the energies using symmetrization at $J/Q = 0$ and 0.1 are -0.77812 and -0.83694 , respectively, slightly lower than -0.77806 and -0.83688 without symmetrization, with a difference around 0.00006. For $L \leq 16$, with and without symmetrization, the energy differences are also as small as 0.00002. In all these cases, we find magnetization and dimerization have no visible changes with and without symmetrization, which is similar to the study of the Heisenberg model [70]. The comparison about symmetrization indicates our obtained PEPS is well optimized as a good ground state that can well respect the lattice and spin symmetry.

In Table II, we summarize the physical quantities obtained from QMC and PEPS. It is clear that the obtained physical quantities including energies, magnetization, and dimerization from PEPS are in excellent agreement with those from QMC across different system sizes, and the energy differences can be as small as 0.00009 on 20×20 sites. These results show that $D = 8$ PEPS can produce well converged results up to 20×20 sites, and demonstrate the extraordinary capability of PEPS in handling near critical systems.

2. comparison with DMRG and convergence

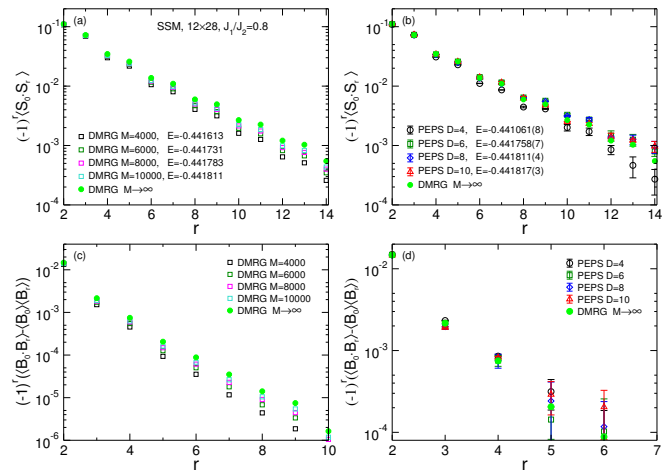


Figure S1. Ground-state energy, spin, and dimer correlation functions from the DMRG and PEPS simulations on the 12×28 SSM at $J_1/J_2 = 0.8$. M is the number of SU(2) multiplets in the DMRG simulations with SU(2) symmetry. The correlation functions are measured along the central row $y = 6$. The reference site for spin correlation is chosen at the third column near the left edge. The dimer correlations are measured for the nearest-neighbor bonds along the x direction with the reference bond located between the third and fourth columns.

Now we directly compare the PEPS and DMRG results of the SSM on a long $L_y \times L_x$ strip with $L_y = 12$, $L_x = 28$. Here we focus on $J_1/J_2 = 0.8$ (set $J_2 = 1$), which is close to the critical point and the nature of which is controversial according to previous studies. The strip geometry has open boundary conditions along both the x - and y -directions. The

Table II. Comparison between PEPS and QMC results on $J-Q$ model on open boundary systems, including ground state energies (set $Q = 1$), magnetizations $\langle M_z^2 \rangle$ and dimerizations $\langle D \rangle^2$. In PEPS calculations, Monte Carlo sampling errors are order of 10^{-6} for energies E_{PEPS} and order of 10^{-5} for $\langle M_z^2 \rangle$ and $\langle D \rangle^2$. For QMC results $\beta = 120$ is used, and sampling errors for these quantities are order of 10^{-6} .

$J/Q = 0$							$J/Q = 0.1$					
L	E_{PEPS}	E_{QMC}	$\langle M_z^2 \rangle_{PEPS}$	$\langle M_z^2 \rangle_{QMC}$	$\langle D \rangle_{PEPS}^2$	$\langle D \rangle_{QMC}^2$	E_{PEPS}	E_{QMC}	$\langle M_z^2 \rangle_{PEPS}$	$\langle M_z^2 \rangle_{QMC}$	$\langle D \rangle_{PEPS}^2$	$\langle D \rangle_{QMC}^2$
6	-0.66172	-0.66174	0.02531(8)	0.02539	0.00572(2)	0.00565	-0.71708	-0.71711	0.02665(6)	0.02672	0.00533(2)	0.00526
8	-0.70379	-0.70383	0.01565(9)	0.01573	0.00433(2)	0.00430	-0.76015	-0.76019	0.01670(3)	0.01684	0.00396(1)	0.00392
10	-0.72897	-0.72903	0.01074(6)	0.01092	0.00355(1)	0.00349	-0.78603	-0.78608	0.01175(3)	0.01187	0.00316(0)	0.00312
12	-0.74558	-0.74564	0.00804(4)	0.00812	0.00298(3)	0.00295	-0.80318	-0.80322	0.00890(4)	0.00898	0.00262(1)	0.00258
14	-0.75735	-0.75739	0.00633(2)	0.00634	0.00260(1)	0.00256	-0.81534	-0.81539	0.00704(4)	0.00712	0.00224(2)	0.00219
16	-0.76606	-0.76613	0.00507(3)	0.00513	0.00231(2)	0.00227	-0.82440	-0.82446	0.00577(3)	0.00585	0.00194(1)	0.00191
20	-0.77812	-0.77820	0.00353(2)	0.00360	0.00192(1)	0.00186	-0.83694	-0.83703	0.00412(3)	0.00424	0.00157(1)	0.00151

DMRG simulations with spin SU(2) symmetry use a maximum bond dimension of $M = 10000$ SU(2) multiplets, which is equivalent to about 40000 U(1) states and ensures a good convergence with the truncation error at about 1×10^{-6} . The ground-state energy per site for each M is listed in the legend of Fig. S1(a). The DMRG correlation functions are measured along the central row ($y = 6$) and are extrapolated versus $1/M$ ($M = 4000 - 10000$) following a second order polynomial fit. The extrapolated results are shown by the green filled circles in Figs. S1(a) and S1(c). For the spin correlation function $\langle \mathbf{S}_0 \cdot \mathbf{S}_r \rangle$, the reference site \mathbf{S}_0 is chosen at the third column near the left edge. For the dimer correlation function $\langle B_0 B_r \rangle - \langle B_0 \rangle \langle B_r \rangle$, the bond operators are chosen along the x direction, namely $B_r = \mathbf{S}_r \cdot \mathbf{S}_{r+\hat{x}}$ (\hat{x} is the unit vector along the x direction). The reference bond for dimer correlations is chosen between the third and fourth columns near the left boundary.

The PEPS results from $D = 4 - 10$ are also presented to compare with the DMRG results. Firstly, we note that the PEPS energies at $D = 8$ and 10 agree very well with the $M = 10000$ DMRG energy. Meanwhile, the converged PEPS correlations also agree very well with those obtained from DMRG, as shown in Figs. S1(b) and S1(d). These comparisons further demonstrate the accuracy of our PEPS results. It also shows that the PEPS simulations with $D = 8$ are good enough to converge the results for the 12×28 SSM.

Here we explicitly show the convergence of energy and order parameters on the largest available 20×20 SSM system at $J_1/J_2 = 0.8$, shown in Table. III. In the calculations, for the order parameters $\langle M^2 \rangle$ and $\langle Q^2 \rangle$ defined based on correlation functions, all pairs of spin and dimer correlations are computed for summation, respectively. Other order parameters mainly involve local terms, which have less computational cost and can be obtained with smaller sampling uncertainty, allowing to check the convergence in higher accuracy. Similar to 12×28 , for 20×20 we can see visible improvement by increasing $D = 4$ to $D = 8$, and the $D = 6$ results are rather close to $D = 8$ results. Further increasing D to 10, the results almost have no further visible improvement, indicating $D = 8$ indeed converges well for the physical quantities. Actually, it has also been shown that the $D = 8$ PEPS simulations can converge quite well for other highly frustrated spin models [46–48], including the J_1 - J_2 - J_3 model up to 20×28 sites [47], as well as the above highly nontrivial

$J - Q$ model. In the meanwhile, in Table. III, we can see for large D it has $\langle M^2 \rangle = 3\langle M_z^2 \rangle$ and $\langle M_z \rangle$ is almost zero within the Monte Carlo sampling error where $M_z = \frac{1}{L^2} \sum_{i_x, i_y} (-1)^{i_x + i_y} S_{i_x, i_y}^z$, indicating the SU(2) symmetry of the ground state recovers very well.

3. comparison with iPEPS and iPESS

We conduct a comparison of energy per site between the finite PEPS and iPEPS methods, shown in Fig. S2. For this purpose, we utilize the best iPEPS energies reported in Ref. [52] at $J_1/J_2 = 0.75, 0.76, 0.77,$ and 0.78 , all obtained with a bond dimension of $D = 10$. To obtain the thermodynamic limit energy for our finite size calculations, we perform an extrapolation of the finite PEPS energy using systems with sizes ranging from $L = 6$ to $L = 20$. To facilitate finite-size scaling, one can choose different central cluster $\tilde{L} \times \tilde{L}$ for finite-size scaling [46, 47, 70], as depicted in Fig. S2. Regardless of the chosen central cluster, the extrapolated energies for each J_1/J_2 remain almost identical, similar to previous studies [46, 47, 70]. These extrapolated PEPS energies and iPEPS energies show a nice agreement with up to 5 significant digits.

We also compare the SSM energies at $J_1/J_2 = 0.8$ with other available results, here from the infinite-size projected entangled simplex states (iPESS) results, shown in Fig. S3. The best iPESS result ($D = 7$) is taken from Ref. [52]. We can see the extrapolated finite PEPS energies also agree well with the iPESS results up to 4 significant digits.

Similar to the iPEPS analysis in Ref. [52], we can determine the first-order transition point between the DVBS (dimer valence-bond solid) and PVBS (plaquette valence-bond solid) phases by examining the ground state energy. The DVBS phase corresponds to a dimer state with an exact energy $E_{DVBS} = -0.375$. Using finite size scaling, we can get the thermodynamic limit energies at $J_1/J_2 = 0.68$ and 0.72 , and estimate the energies at other J_1/J_2 points with a presumed linear extrapolation with respect to J_1/J_2 (a linear assumption is reasonable as the energy seems to change linearly in a large range of J_1/J_2 according to our results or previous studies [52, 54, 56]). The energy variation about J_1/J_2 , obviously suggests a first-order DVBS-PVBS transition at $J_1/J_2 \approx 0.676$, shown in Fig. S4, which is also in good

Table III. The convergence of energy and order parameters with respect to the PEPS bond dimension D on the 20×20 SSM system at $J_1/J_2 = 0.8$ (set $J_2 = 1$). $\langle P \rangle^2$, $\langle D \rangle^2$ and $\langle Q \rangle^2$ are all valid VBS order parameters, used for cross check; $\langle M^2 \rangle$ are AFM order parameters, and $3\langle M_z^2 \rangle$ and $\langle M_z \rangle$ are used to check the SU(2) symmetry.

D	E	$\langle P \rangle^2$	$\langle D \rangle^2$	$\langle Q \rangle^2$	$\langle M^2 \rangle$	$3\langle M_z^2 \rangle$	$\langle M_z \rangle$
4	-0.442104(8)	0.01624(8)	0.01738(9)	0.0380(2)	0.0139(1)	0.01450(9)	0.0014(4)
6	-0.442861(9)	0.01349(5)	0.01454(5)	0.0324(1)	0.0158(1)	0.01571(9)	0.0011(5)
8	-0.442920(2)	0.01341(8)	0.01442(9)	0.0321(2)	0.0155(1)	0.01548(6)	0.0001(5)
10	-0.442928(3)	0.01344(9)	0.01441(5)	0.0320(1)	0.0155(2)	0.01549(5)	0.0003(4)

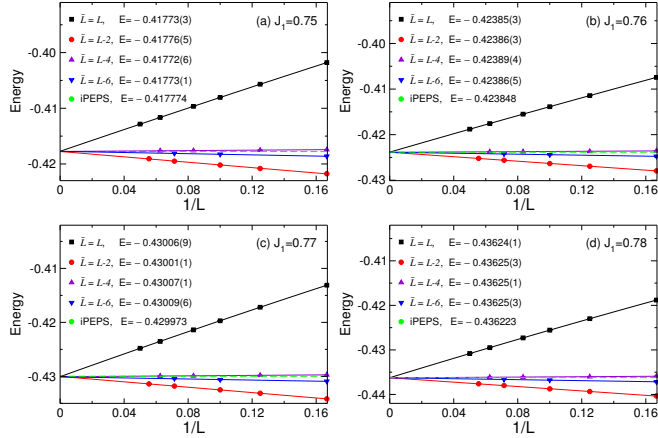


Figure S2. Finite size scaling of ground state energies with $L = 6 - 20$ for SSM at different J_1 . The iPEPS results are from Ref. [52]. For $\tilde{L} = L$ second-order polynomial fits are used and for other cases, linear fits are used. Extrapolated thermodynamic limit energies are listed in the legend.

agreement with the iPEPS and iPESS results, as well as the DMRG study [54].

4. PVBS-AFM transition point

We now examine the PVBS-AFM phase transition point in the SSM determined by various methods, which is very challenging for accurate determination. The outcomes of the DMRG investigation conducted on an infinitely long cylinder (L_x is infinite while $L_y = L$ is finite) show apparent finite-size effects [54]. The observed values of $J_1^c(L)$ are 0.693, 0.728, 0.762, and 0.77 for L equaling 6, 8, 10, and 12, respectively [54]. Extrapolating to the 2D limit, the transition point is estimated as $J_1^c = 0.85(1)$ (linear fit $1/L$ with L ranging from 6 to 12) or $J_1^c = 0.81$ (linear fit $1/L$ with L ranging from 10 to 12), as illustrated in Fig. S5. On the other hand, based on the singlet minimum points from the later DMRG study [57] ($L_x = 2L$ is finite), the estimation of g_{c1} with similar linear fits can also be 0.834(4) for $L = 6 - 12$ and 0.818 for $L = 10 - 12$ [see Fig. S5], rather close to $g_{c2} \approx 0.82 \sim 0.83$ [57, 59]. This indicates the possibility that g_{c1} and g_{c2} coincide, and the proposed narrow spin liquid might be a consequence of finite-size effects. Noticeably, these estimations based on different cylindrical systems and different physical quantities, seemingly reach an point around

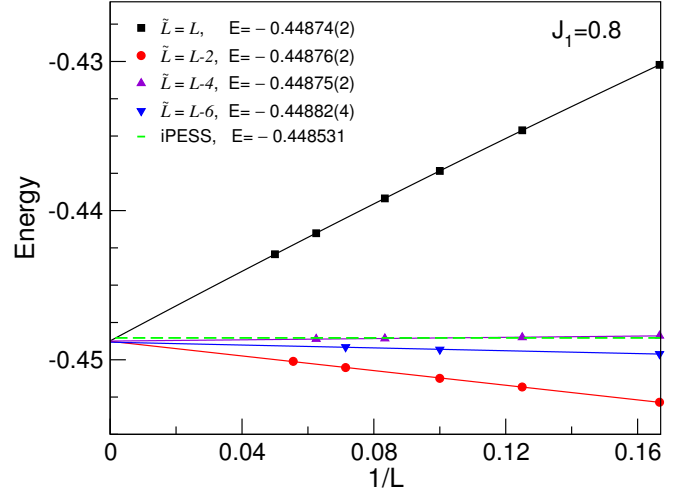


Figure S3. Finite size scaling of ground state energies with $L = 6 - 20$ for SSM at $J_1 = 0.8$. The iPESS results are from Ref. [56]. For $\tilde{L} = L$ second-order polynomial fits are used and for other cases, linear fits are used. Extrapolated thermodynamic limit energies are listed in the legend.

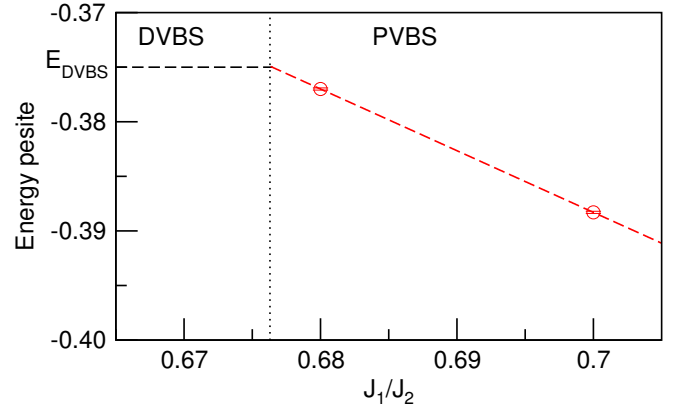


Figure S4. Energy variation with respect to J_1/J_2 for the SSM. Red points denote thermodynamic limit energies at $J_1/J_2 = 0.68$ and 0.72, and red dashed line denotes a presumed linear change of the energies close to the first-order transition point.

$J_1 \sim 0.82$ in the 2D limit, closely resembling our obtained PVBS-AFM transition point, $J_1^c = 0.828(5)$.

Additionally, the PVBS-AFM phase transition points from infinite tensor network methods are a bit different from our $J_1^c = 0.828(5)$, which are $J_1^c = 0.765(15)$ [52] or 0.79 [56].

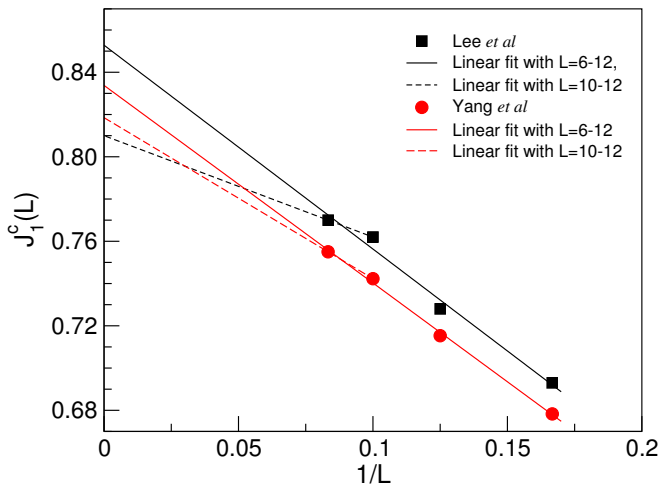


Figure S5. Finite-size extrapolations of the relevant points of the DMRG results from Ref. [54] (black) and Ref. [57] (red). They use different systems and physical quantities to locate the turning points, so their values for a given cylinder width L could be different. Linear fits with $L = 6 - 12$ and $L = 10 - 12$ are shown, which give extrapolated values 0.85(1) and 0.81 using the results from Ref. [54] and, 0.834(4) and 0.818 using singlet minimum results from Ref. [57], respectively.

Generally speaking, finite PEPS methods suffer finite size effects (the finite- D effects can be removed by a mild D for a moderate system size, e.g. here $D = 8$ for 20×20), and infinite tensor network methods suffer finite D effects. In our finite-size calculations, the uncertainty caused by finite-size effects for the PVBS-AFM transition point has been significantly reduced by crosschecking different physical quantities including the order parameter ratio that is related to emergent symmetry. For infinite-size tensor network simulations, we believe a proper consideration about finite D effects may also give the similar result. We point out that for larger finite-size systems larger D is necessary for convergence, and the systematical investigation of finite- L and finite- D effects can be found in Refs. [93, 94].

Appendix S-2: Setup for open boundary systems

In open boundary systems, the presence of boundaries will induce dimerized patterns, which requires careful consideration about such effects on the real plaquette pattern in the PVBS phase. To illustrate this, we examine the Shastry-Sutherland model (SSM) and calculate the values of local plaquette operators at each site.

We start by considering setup A, where diagonal interaction terms exist at the corners. We consider an $L \times L$ lattice with $L = 20$. We observe a distinct plaquette pattern near the boundaries of the systems, but it becomes blurry in the middle region, shown in Fig. S6(a). This blurriness is a consequence of the boundaries. Specifically, the x -directional boundaries induce a certain pattern, while the y -directional boundaries give rise to another kind of plaquette pattern. The 'superposition' of these equal-footing boundary effects results in the formation of domain walls along the diagonal directions [see Fig. S6(a)]. However, if the x - and y -boundaries are not treated on equal footing, a clear plaquette pattern may eventually emerge in the middle region, as illustrated in Fig. S6(b) for a 16×28 system.

In setup A, the presence of domain walls poses a challenge for finite-size scaling since the VBS order parameters defined on the entire lattice are not well-defined due to the incompatibility of the plaquette pattern in different domains. For example, considering the boundary-induced plaquette order parameter $P = \frac{1}{N_p} \sum_i (-1)^{i_x} \Pi_i$, the contributions from different domains could be partly canceled (so is the VBS order parameters based on bond-bond correlations). Even if one attempts to define the VBS order parameters within a specific domain, the ambiguity caused by the domain walls cannot be entirely removed.

The plaquette pattern in the middle region of 16×28 system using setup A [Fig. S6(b)], suggests one should use the setup B, where corner sites have no diagonal interaction terms. In this context, the plaquette pattern is compatible with the boundaries [see Fig. S6(c)]. As a result, there are no domain walls, and the VBS order parameters can be defined unambiguously over the lattice, which ensures a more reliable and consistent analysis of the VBS order parameters. Consequently, throughout this work, setup B is used to compute all physical quantities in the SSM and the extended SSM.

-
- [1] H. Kageyama, K. Yoshimura, R. Stern, N. V. Mushnikov, K. Onizuka, M. Kato, K. Kosuge, C. P. Slichter, T. Goto, and Y. Ueda, "Exact dimer ground state and quantized magnetization plateaus in the two-dimensional spin system $\text{SrCu}_2(\text{BO}_3)_2$," *Phys. Rev. Lett.* **82**, 3168–3171 (1999).
- [2] Tsutomu Momoi and Keisuke Totsuka, "Magnetization plateaus of the shastry-sutherland model for $\text{SrCu}_2(\text{BO}_3)_2$: Spin-density wave, supersolid, and bound states," *Phys. Rev. B* **62**, 15067–15078 (2000).
- [3] K. Kodama, M. Takigawa, M. Horvatić, C. Berthier, H. Kageyama, Y. Ueda, S. Miyahara, F. Becca, and F. Mila,

- "Magnetic superstructure in the two-dimensional quantum antiferromagnet $\text{SrCu}_2(\text{BO}_3)_2$," *Science* **298**, 395–399 (2002).
- [4] Kenzo Onizuka, Hiroshi Kageyama, Yasuo Narumi, Koichi Kindo, Yutaka Ueda, and Tsuneaki Goto, "1/3 magnetization plateau in $\text{SrCu}_2(\text{BO}_3)_2$ -stripe order of excited triplets," *Journal of the Physical Society of Japan* **69**, 1016–1018 (2000).
- [5] M Takigawa, K Kodama, M Horvatić, C Berthier, H Kageyama, Y Ueda, S Miyahara, Federico Becca, and F Mila, "The 1/8-magnetization plateau state in the 2d quantum antiferromagnet $\text{SrCu}_2(\text{BO}_3)_2$: spin superstructure, phase transition, and spin dynamics studied by high-field nmr," *Physica B: Condensed*

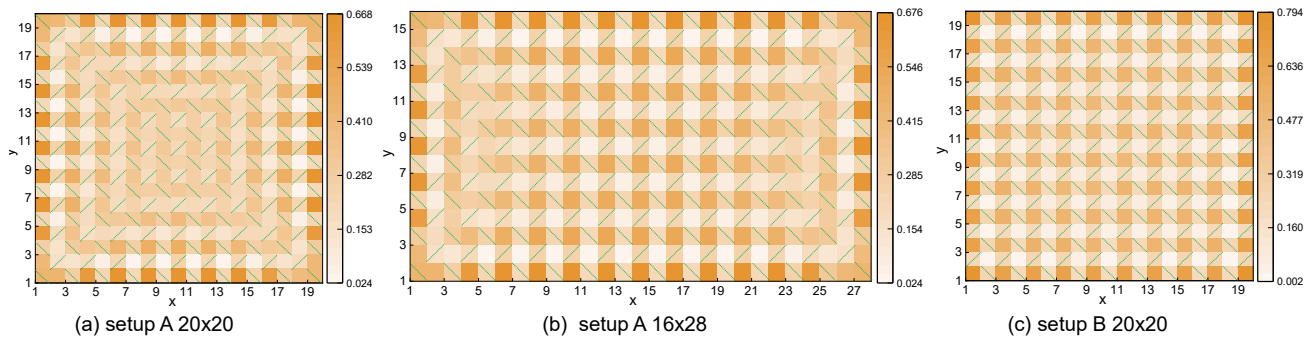


Figure S6. Two setups for the SSM. Green diagonal line denote diagonal interaction terms. Corner sites have diagonal interaction terms in setup A and but not in setup B. (a-b) show the plaquette operator values Π_i setup A on 20×20 and 16×28 systems. (c) shows the plaquette values on 20×20 using setup B. All three cases use $J_1/J_2 = 0.74$.

- Matter* **346**, 27–33 (2004).
- [6] K. P. Schmidt, J. Dorier, A. M. Läuchli, and F. Mila, “Supersolid phase induced by correlated hopping in spin-1/2 frustrated quantum magnets,” *Phys. Rev. Lett.* **100**, 090401 (2008).
- [7] F. Levy, I. Sheikin, C. Berthier, M. Horvatić, M. Takigawa, H. Kageyama, T. Waki, and Y. Ueda, “Field dependence of the quantum ground state in the shastry-sutherland system $\text{SrCu}_2(\text{BO}_3)_2$,” *Europhysics Letters* **81**, 67004 (2008).
- [8] Suchitra E. Sebastian, N. Harrison, P. Sengupta, C. D. Batista, S. Francoual, E. Palm, T. Murphy, N. Marcano, H. A. Dabkowska, and B. D. Gaulin, “Fractalization drives crystalline states in a frustrated spin system,” *Proceedings of the National Academy of Sciences* **105**, 20157–20160 (2008).
- [9] Marcelo Jaime, Ramzy Daou, Scott A. Crooker, Franziska Weickert, Atsuko Uchida, Adrian E. Feiguin, Cristian D. Batista, Hanna A. Dabkowska, and Bruce D. Gaulin, “Magnetostriction and magnetic texture to 100.75 tesla in frustrated $\text{SrCu}_2(\text{BO}_3)_2$,” *Proceedings of the National Academy of Sciences* **109**, 12404–12407 (2012).
- [10] M. Takigawa, M. Horvatić, T. Waki, S. Krämer, C. Berthier, F. Lévy-Bertrand, I. Sheikin, H. Kageyama, Y. Ueda, and F. Mila, “Incomplete devil’s staircase in the magnetization curve of $\text{SrCu}_2(\text{BO}_3)_2$,” *Phys. Rev. Lett.* **110**, 067210 (2013).
- [11] Y. H. Matsuda, N. Abe, S. Takeyama, H. Kageyama, P. Corboz, A. Honecker, S. R. Manmana, G. R. Foltin, K. P. Schmidt, and F. Mila, “Magnetization of $\text{SrCu}_2(\text{BO}_3)_2$ in ultrahigh magnetic fields up to 118 t,” *Phys. Rev. Lett.* **111**, 137204 (2013).
- [12] S. Haravifard, D. Graf, A.E. Feiguin, C.D. Batista, J.C. Lang, D.M. Silevitch, G. Srajer, B.D. Gaulin, H.A. Dabkowska, and T.F. Rosenbaum, “Crystallization of spin superlattices with pressure and field in the layered magnet $\text{SrCu}_2(\text{BO}_3)_2$,” *Nature communications* **7**, 11956 (2016).
- [13] Siddharth A Parameswaran, Ari M Turner, Daniel P Arovas, and Ashvin Vishwanath, “Topological order and absence of band insulators at integer filling in non-symmorphic crystals,” *Nature Physics* **9**, 299–303 (2013).
- [14] Judit Romhányi, Karlo Penc, and Ramachandran Ganesh, “Hall effect of triplons in a dimerized quantum magnet,” *Nature Communications* **6**, 6805 (2015).
- [15] Paul A. McClarty, F. Krüger, Tatiana Guidi, S.F. Parker, Keith Refson, A.W. Parker, Dharmalingam Prabhakaran, and Radu Coldea, “Topological triplon modes and bound states in a shastry–sutherland magnet,” *Nature Physics* **13**, 736–741 (2017).
- [16] Dirk Wulferding, Youngsu Choi, Seungyeol Lee, Mikhail A Prosnikov, Yann Gallais, Peter Lemmens, Chengchao Zhong, Hiroshi Kageyama, and Kwang-Yong Choi, “Thermally populated versus field-induced triplon bound states in the shastry-sutherland lattice $\text{SrCu}_2(\text{BO}_3)_2$,” *npj Quantum Materials* **6**, 102 (2021).
- [17] T. Senthil, Ashvin Vishwanath, Leon Balents, Subir Sachdev, and Matthew P. A. Fisher, “Deconfined quantum critical points,” *Science* **303**, 1490–1494 (2004).
- [18] T. Senthil, Leon Balents, Subir Sachdev, Ashvin Vishwanath, and Matthew P. A. Fisher, “Quantum criticality beyond the landau-ginzburg-wilson paradigm,” *Phys. Rev. B* **70**, 144407 (2004).
- [19] M. E. Zayed, Ch. Rüegg, A. M. Läuchli, C. Panagopoulos, S. S. Saxena, M. Ellerby, D. F. McMorrow, Th. Strässle, S. Klotz, G. Hamel, *et al.*, “4-spin plaquette singlet state in the Shastry–Sutherland compound $\text{SrCu}_2(\text{BO}_3)_2$,” *Nat. Phys.* **13**, 962–966 (2017).
- [20] Jing Guo, Guangyu Sun, Bowen Zhao, Ling Wang, Wenshan Hong, Vladimir A. Sidorov, Nvsen Ma, Qi Wu, Shiliang Li, Zi Yang Meng, Anders W. Sandvik, and Liling Sun, “Quantum phases of $\text{SrCu}_2(\text{BO}_3)_2$ from high-pressure thermodynamics,” *Phys. Rev. Lett.* **124**, 206602 (2020).
- [21] Olexei I. Motrunich and Ashvin Vishwanath, “Emergent photons and transitions in the $O(3)$ sigma model with hedgehog suppression,” *Phys. Rev. B* **70**, 075104 (2004).
- [22] Yizhi You and Yi-Zhuang You, “Stripe melting and a transition between weak and strong symmetry protected topological phases,” *Phys. Rev. B* **93**, 195141 (2016).
- [23] Chong Wang, Adam Nahum, Max A. Metlitski, Cenke Xu, and T. Senthil, “Deconfined quantum critical points: Symmetries and dualities,” *Phys. Rev. X* **7**, 031051 (2017).
- [24] Max A. Metlitski and Ryan Thorngren, “Intrinsic and emergent anomalies at deconfined critical points,” *Phys. Rev. B* **98**, 085140 (2018).
- [25] Chao-Ming Jian, Alex Thomson, Alex Rasmussen, Zhen Bi, and Cenke Xu, “Deconfined quantum critical point on the triangular lattice,” *Phys. Rev. B* **97**, 195115 (2018).
- [26] Anders W. Sandvik, “Evidence for deconfined quantum criticality in a two-dimensional Heisenberg model with four-spin interactions,” *Phys. Rev. Lett.* **98**, 227202 (2007).
- [27] Roger G. Melko and Ribhu K. Kaul, “Scaling in the fan of an unconventional quantum critical point,” *Phys. Rev. Lett.* **100**, 017203 (2008).
- [28] F-J Jiang, M Nyfeler, S Chandrasekharan, and U-J Wiese,

- “From an antiferromagnet to a valence bond solid: evidence for a first-order phase transition,” *Journal of Statistical Mechanics: Theory and Experiment* **2008**, P02009 (2008).
- [29] Jie Lou, Anders W. Sandvik, and Naoki Kawashima, “Antiferromagnetic to valence-bond-solid transitions in two-dimensional $SU(N)$ Heisenberg models with multispin interactions,” *Phys. Rev. B* **80**, 180414 (2009).
- [30] Adam Nahum, P. Serna, J. T. Chalker, M. Ortuño, and A. M. Somoza, “Emergent $SO(5)$ symmetry at the néel to valence-bond-solid transition,” *Phys. Rev. Lett.* **115**, 267203 (2015).
- [31] D. Charrier and F. Alet, “Phase diagram of an extended classical dimer model,” *Phys. Rev. B* **82**, 014429 (2010).
- [32] Anders W. Sandvik, “Continuous quantum phase transition between an antiferromagnet and a valence-bond solid in two dimensions: Evidence for logarithmic corrections to scaling,” *Phys. Rev. Lett.* **104**, 177201 (2010).
- [33] Ribhu K. Kaul, “Quantum criticality in $SU(3)$ and $SU(4)$ antiferromagnets,” *Phys. Rev. B* **84**, 054407 (2011).
- [34] Matthew S. Block, Roger G. Melko, and Ribhu K. Kaul, “Fate of $\mathbb{C}P^{N-1}$ fixed points with q monopoles,” *Phys. Rev. Lett.* **111**, 137202 (2013).
- [35] Kenji Harada, Takafumi Suzuki, Tsuyoshi Okubo, Haruhiko Matsuo, Jie Lou, Hiroshi Watanabe, Syngye Todo, and Naoki Kawashima, “Possibility of deconfined criticality in $su(n)$ heisenberg models at small n ,” *Phys. Rev. B* **88**, 220408 (2013).
- [36] Kun Chen, Yuan Huang, Youjin Deng, A. B. Kuklov, N. V. Prokof'ev, and B. V. Svistunov, “Deconfined criticality flow in the heisenberg model with ring-exchange interactions,” *Phys. Rev. Lett.* **110**, 185701 (2013).
- [37] Sumiran Pujari, Fabien Alet, and Kedar Damle, “Transitions to valence-bond solid order in a honeycomb lattice antiferromagnet,” *Phys. Rev. B* **91**, 104411 (2015).
- [38] Adam Nahum, J. T. Chalker, P. Serna, M. Ortuño, and A. M. Somoza, “Deconfined quantum criticality, scaling violations, and classical loop models,” *Phys. Rev. X* **5**, 041048 (2015).
- [39] Hui Shao, Wenan Guo, and Anders W. Sandvik, “Quantum criticality with two length scales,” *Science* **352**, 213–216 (2016).
- [40] G. J. Sreejith, Stephen Powell, and Adam Nahum, “Emergent $SO(5)$ symmetry at the columnar ordering transition in the classical cubic dimer model,” *Phys. Rev. Lett.* **122**, 080601 (2019).
- [41] F. F. Assaad and Tarun Grover, “Simple fermionic model of deconfined phases and phase transitions,” *Phys. Rev. X* **6**, 041049 (2016).
- [42] Toshihiro Sato, Martin Hohenadler, and Fakher F. Assaad, “Dirac fermions with competing orders: Non-Landau transition with emergent symmetry,” *Phys. Rev. Lett.* **119**, 197203 (2017).
- [43] Yi-Zhuang You, Yin-Chen He, Cenke Xu, and Ashvin Vishwanath, “Symmetric fermion mass generation as deconfined quantum criticality,” *Phys. Rev. X* **8**, 011026 (2018).
- [44] Xue-Feng Zhang, Yin-Chen He, Sebastian Eggert, Roderich Moessner, and Frank Pollmann, “Continuous easy-plane deconfined phase transition on the kagome lattice,” *Phys. Rev. Lett.* **120**, 115702 (2018).
- [45] Y. Liu, Z. Wang, T. Sato, M. Hohenadler, C. Wang, W. Guo, and F.F. Assaad, “Superconductivity from the condensation of topological defects in a quantum spin-Hall insulator,” *Nat Commun* **10**, 2658 (2019).
- [46] Wen-Yuan Liu, Shou-Shu Gong, Yu-Bin Li, Didier Poilblanc, Wei-Qiang Chen, and Zheng-Cheng Gu, “Gapless quantum spin liquid and global phase diagram of the spin-1/2 $J_1 - J_2$ square antiferromagnetic Heisenberg model,” *Science Bulletin* **67**, 1034–1041 (2022).
- [47] Wen-Yuan Liu, Juraj Hasik, Shou-Shu Gong, Didier Poilblanc, Wei-Qiang Chen, and Zheng-Cheng Gu, “Emergence of gapless quantum spin liquid from deconfined quantum critical point,” *Phys. Rev. X* **12**, 031039 (2022).
- [48] Wen-Yuan Liu, Shou-Shu Gong, Wei-Qiang Chen, and Zheng-Cheng Gu, “Emergent symmetry in quantum phase transition: From deconfined quantum critical point to gapless quantum spin liquid,” *Science Bulletin* **69**, 190–196 (2024).
- [49] Yi Cui, Lu Liu, Huihang Lin, Kai-Hsin Wu, Wenshan Hong, Xuefei Liu, Cong Li, Ze Hu, Ning Xi, Shiliang Li, Rong Yu, Anders W. Sandvik, and Weiqiang Yu, “Proximate deconfined quantum critical point in $SrCu_2(BO_3)_2$,” *Science* **380**, 1179–1184 (2023).
- [50] B. Sriram Shastry and Bill Sutherland, “Exact ground state of a quantum mechanical antiferromagnet,” *Physica B+C* **108**, 1069–1070 (1981).
- [51] Shin Miyahara and Kazuo Ueda, “Exact dimer ground state of the two dimensional heisenberg spin system $SrCu_2(BO_3)_2$,” *Phys. Rev. Lett.* **82**, 3701–3704 (1999).
- [52] Philippe Corboz and Frédéric Mila, “Tensor network study of the Shastry-Sutherland model in zero magnetic field,” *Phys. Rev. B* **87**, 115144 (2013).
- [53] C. Boos, S. P. G. Crone, I. A. Niesen, P. Corboz, K. P. Schmidt, and F. Mila, “Competition between intermediate plaquette phases in $SrCu_2(BO_3)_2$ under pressure,” *Phys. Rev. B* **100**, 140413 (2019).
- [54] Jong Yeon Lee, Yi-Zhuang You, Subir Sachdev, and Ashvin Vishwanath, “Signatures of a deconfined phase transition on the Shastry-Sutherland lattice: Applications to quantum critical $SrCu_2(BO_3)_2$,” *Phys. Rev. X* **9**, 041037 (2019).
- [55] Tokuro Shimokawa, “Signatures of finite-temperature mirror symmetry breaking in the $S=\frac{1}{2}$ Shastry-Sutherland model,” *Phys. Rev. B* **103**, 134419 (2021).
- [56] Ning Xi, Hongyu Chen, ZY Xie, and Rong Yu, “First-order transition between the plaquette valence bond solid and antiferromagnetic phases of the Shastry-Sutherland model,” *arXiv:2111.07368* (2021).
- [57] Jianwei Yang, Anders W. Sandvik, and Ling Wang, “Quantum criticality and spin liquid phase in the Shastry-Sutherland model,” *Phys. Rev. B* **105**, L060409 (2022).
- [58] Ahmet Keleş and Erhai Zhao, “Rise and fall of plaquette order in the Shastry-Sutherland magnet revealed by pseudofermion functional renormalization group,” *Phys. Rev. B* **105**, L041115 (2022).
- [59] Ling Wang, Yalei Zhang, and Anders W Sandvik, “Quantum spin liquid phase in the Shastry-Sutherland model detected by an improved level spectroscopic method,” *Chinese Physics Letters* **39**, 077502 (2022).
- [60] Junsen Wang, Han Li, Ning Xi, Yuan Gao, Qing-Bo Yan, Wei Li, and Gang Su, “Plaquette singlet transition, magnetic barocaloric effect, and spin supersolidity in the shastry-sutherland model,” *Phys. Rev. Lett.* **131**, 116702 (2023).
- [61] Zhenzhong Shi, Sachith Dissanayake, Philippe Corboz, William Steinhardt, David Graf, DM Silevitch, Hanna A Dabkowska, TF Rosenbaum, Frédéric Mila, and Sara Haravifard, “Discovery of quantum phases in the Shastry-Sutherland compound $SrCu_2(BO_3)_2$ under extreme conditions of field and pressure,” *Nature Communications* **13**, 2301 (2022).
- [62] J Larrea Jiménez, SPG Crone, Ellen Fogh, Mohamed Ezzat Zayed, Rolf Lortz, Ekaterina Pomjakushina, Kaziemerzh Conder, Andreas M Läuchli, Lukas Weber, Stefan Wessel, *et al.*, “A quantum magnetic analogue to the critical point of water,” *Nature* **592**, 370–375 (2021).
- [63] Akihisa Koga and Norio Kawakami, “Quantum phase transi-

- tions in the Shastry-Sutherland model for $\text{SrCu}_2(\text{BO}_3)_2$,” *Phys. Rev. Lett.* **84**, 4461–4464 (2000).
- [64] Yoshihiro Takushima, Akihisa Koga, and Norio Kawakami, “Competing spin-gap phases in a frustrated quantum spin system in two dimensions,” *Journal of the Physical Society of Japan* **70**, 1369–1374 (2001).
- [65] Oleg A. Starykh, Akira Furusaki, and Leon Balents, “Anisotropic pyrochlores and the global phase diagram of the checkerboard antiferromagnet,” *Phys. Rev. B* **72**, 094416 (2005).
- [66] R. F. Bishop, P. H. Y. Li, D. J. J. Farnell, J. Richter, and C. E. Campbell, “Frustrated heisenberg antiferromagnet on the checkerboard lattice: J_1 - J_2 model,” *Phys. Rev. B* **85**, 205122 (2012).
- [67] Haiyuan Zou, Fan Yang, and Wei Ku, “Nearly degenerate ground states of a checkerboard antiferromagnet and their bosonic interpretation,” [arXiv:2011.06520](https://arxiv.org/abs/2011.06520) (2020).
- [68] Wen-Yuan Liu, Shao-Jun Dong, Yong-Jian Han, Guang-Can Guo, and Lixin He, “Gradient optimization of finite projected entangled pair states,” *Phys. Rev. B* **95**, 195154 (2017).
- [69] Wen-Yuan Liu, Shaojun Dong, Chao Wang, Yongjian Han, Hong An, Guang-Can Guo, and Lixin He, “Gapless spin liquid ground state of the spin-1/2 J_1 - J_2 Heisenberg model on square lattices,” *Phys. Rev. B* **98**, 241109 (2018).
- [70] Wen-Yuan Liu, Yi-Zhen Huang, Shou-Shu Gong, and Zheng-Cheng Gu, “Accurate simulation for finite projected entangled pair states in two dimensions,” *Phys. Rev. B* **103**, 235155 (2021).
- [71] See Supplemental Material including Refs. [89–94], for additional information about the comparison with other methods and the convergence behaviour about bond dimension D .
- [72] Bowen Zhao, Phillip Weinberg, and Anders W Sandvik, “Symmetry-enhanced discontinuous phase transition in a two-dimensional quantum magnet,” *Nature Physics* **15**, 678–682 (2019).
- [73] Pablo Serna and Adam Nahum, “Emergence and spontaneous breaking of approximate $O(4)$ symmetry at a weakly first-order deconfined phase transition,” *Phys. Rev. B* **99**, 195110 (2019).
- [74] Anders W. Sandvik, “Computational studies of quantum spin systems,” *AIP Conference Proceedings* **1297**, 135–338 (2010).
- [75] Xiangjian Qian and Mingpu Qin, “Absence of spin liquid phase in the J_1 - J_2 heisenberg model on the square lattice,” *Phys. Rev. B* **109**, L161103 (2024).
- [76] Philippe Corboz, Piotr Czarnecki, Geert Kapteijns, and Luca Tagliacozzo, “Finite correlation length scaling with infinite projected entangled-pair states,” *Phys. Rev. X* **8**, 031031 (2018).
- [77] Michael Rader and Andreas M. Läuchli, “Finite correlation length scaling in Lorentz-invariant gapless iPEPS wave functions,” *Phys. Rev. X* **8**, 031030 (2018).
- [78] Bram Vanhecke, Juraj Hasik, Frank Verstraete, and Laurens Vanderstraeten, “Scaling hypothesis for projected entangled-pair states,” *Phys. Rev. Lett.* **129**, 200601 (2022).
- [79] H. J. Liao, Z. Y. Xie, J. Chen, Z. Y. Liu, H. D. Xie, R. Z. Huang, B. Normand, and T. Xiang, “Gapless spin-liquid ground state in the $S = 1/2$ kagome antiferromagnet,” *Phys. Rev. Lett.* **118**, 137202 (2017).
- [80] Hiroyuki Nojiri, Hiroshi Kageyama, Kenzo Onizuka, Yutaka Ueda, and Mitsuhiro Motokawa, “Direct observation of the multiple spin gap excitations in two-dimensional dimer system $\text{SrCu}_2(\text{BO}_3)_2$,” *Journal of the Physical Society of Japan* **68**, 2906–2909 (1999).
- [81] T. Röm, D. Hiivonen, U. Nagel, J. Hwang, T. Timusk, and H. Kageyama, “Far-infrared spectroscopy of spin excitations and dzyaloshinskii-moriya interactions in the Shastry-Sutherland compound $\text{SrCu}_2(\text{BO}_3)_2$,” *Phys. Rev. B* **70**, 144417 (2004).
- [82] O. Cépas, K. Kakurai, L. P. Regnault, T. Ziman, J. P. Boucher, N. Aso, M. Nishi, H. Kageyama, and Y. Ueda, “Dzyaloshinskii-moriya interaction in the 2d spin gap system $\text{SrCu}_2(\text{BO}_3)_2$,” *Phys. Rev. Lett.* **87**, 167205 (2001).
- [83] Shin Miyahara and Kazuo Ueda, “Theory of the orthogonal dimer heisenberg spin model for $\text{SrCu}_2(\text{BO}_3)_2$,” *Journal of Physics: Condensed Matter* **15**, R327 (2003).
- [84] K. Kodama, S. Miyahara, M. Takigawa, M. Horvatić, C. Berthier, F. Mila, H. Kageyama, and Y. Ueda, “Field-induced effects of anisotropic magnetic interactions in $\text{SrCu}_2(\text{BO}_3)_2$,” *Journal of Physics: Condensed Matter* **17**, L61 (2005).
- [85] Judit Romhányi, Keisuke Totsuka, and Karlo Penc, “Effect of dzyaloshinskii-moriya interactions on the phase diagram and magnetic excitations of $\text{SrCu}_2(\text{BO}_3)_2$,” *Phys. Rev. B* **83**, 024413 (2011).
- [86] S. Haravifard, A. Banerjee, J. van Wezel, D. M. Silevitch, A. M. dos Santos, J. C. Lang, E. Kermarrec, G. Srajer, B. D. Gaulin, J. J. Molaison, H. A. Dabkowska, and T. F. Rosenbaum, “Emergence of long-range order in sheets of magnetic dimers,” *Proceedings of the National Academy of Sciences* **111**, 14372–14377 (2014).
- [87] Zhenzhong Shi, William Steinhardt, David Graf, Philippe Corboz, Franziska Weickert, Neil Harrison, Marcelo Jaime, Casey Marjerrison, Hanna A Dabkowska, Frédéric Mila, *et al.*, “Emergent bound states and impurity pairs in chemically doped Shastry-Sutherland system,” *Nature Communications* **10**, 2439 (2019).
- [88] T. Nomura, P. Corboz, A. Miyata, S. Zherlitsyn, Y. Ishii, Y. Kohama, YH Matsuda, A. Ikeda, C. Zhong, H. Kageyama, *et al.*, “Unveiling new quantum phases in the Shastry-Sutherland compound $\text{SrCu}_2(\text{BO}_3)_2$ up to the saturation magnetic field,” *Nature Communications* **14**, 3769 (2023).
- [89] F. Verstraete, V. Murg, and J.I. Cirac, “Matrix product states, projected entangled pair states, and variational renormalization group methods for quantum spin systems,” *Advances in Physics* **57**, 143–224 (2008).
- [90] J. Ignacio Cirac, David Pérez-García, Norbert Schuch, and Frank Verstraete, “Matrix product states and projected entangled pair states: Concepts, symmetries, theorems,” *Rev. Mod. Phys.* **93**, 045003 (2021).
- [91] Anders W. Sandvik, “Finite-size scaling and boundary effects in two-dimensional valence-bond solids,” *Phys. Rev. B* **85**, 134407 (2012).
- [92] Tom Viejira, Jutho Haegeman, Frank Verstraete, and Laurens Vanderstraeten, “Direct sampling of projected entangled-pair states,” *Phys. Rev. B* **104**, 235141 (2021).
- [93] Ching-Yu Huang, Sing-Hong Chan, Ying-Jer Kao, and Pochung Chen, “Tensor network based finite-size scaling for two-dimensional ising model,” *Phys. Rev. B* **107**, 205123 (2023).
- [94] Atsushi Ueda and Masaki Oshikawa, “Finite-size and finite bond dimension effects of tensor network renormalization,” *Phys. Rev. B* **108**, 024413 (2023).